Electronic Transitions in Tetrathiafulvalene and Its Radical Cation: A Theoretical Contribution

Rosendo Pou-Amérigo,* Enrique Ortí, Manuela Merchán, Mercedes Rubio, and Pedro M. Viruela

Departament de Química Física, Institut de Ciència Molecular, Universitat de València, Dr. Moliner 50, E−46100 Burjassot (València), Spain

Received: September 27, 2001

The low-lying electronic states of tetrathiafulvalene (TTF) and its radical cation (TTF^+) have been studied using the multistate extension of a multiconfigurational second-order perturbation method (MS−CASPT2). The minimum-energy equilibrium geometries optimized at the CASSCF level have a boatlike conformation for the neutral molecule, with no significant barrier toward planarity. A more aromatic planar structure is, however, found for the ionic system. For TTF, the calculations of the vertical excitation energies comprise valence singlet and triplet states as well as the lowest members of the Rydberg series converging to the first ionization limit. Valence doublet states have been considered for TTF^+. The results obtained lead to elucidate controversial assignments, yielding a full interpretation of the available experimental absorption spectra. In addition, vertical ionization energies of TTF have been computed, and the lowest-energy peaks of the gas-phase photoelectron spectra have been interpreted in the light of the present findings.

1. Introduction

Tetrathiafulvalenes play a fundamental role in the active field of materials technology. It is therefore not surprising that they have been the subject of increasing attention since three decades ago. The prototype of this relevant class of compounds is the tetrathiafulvalene molecule (TTF, see Figure 1). The starting point of the interest can be placed in the early 1970s with the observation of high electrical conductivity in a chloride salt of TTF[1] and the discovery of the metallic behavior exhibited by the charge-transfer complex formed by the donor TTF and the acceptor TCNQ (7,7,8,8-tetracyano-*p*-quinodimethane).[2,3] The TTF-TCNQ complex is actually known as the first true organic metal. In the 80s, after the finding of the first organic superconductors,[4−6] constituted by species related to TTF, the research about TTF-based systems was intensified. Thus, TTF was extensively derivatized in the search for new organic conducting and superconducting solids.[7−10] During the past few years, substituted TTFs have also aroused a growing interest in many other areas of materials chemistry. They have turned out to be extremely versatile building blocks and have found widespread use in the design of novel materials, such as cation sensors, liquid crystals, supramolecular switches and shuttles, redox polymers, photovoltaic devices, and so forth.[11−15]

The reason for such a great variety of applications lies on the unique combination of features that are intrinsic of the TTF system;[12,13] in particular, those concerning its redox behavior are worth emphasizing. The TTF molecule is an effective π-electron donor. It can be oxidized to the cation and subsequently to the dication in a reversible way at low potentials. Moreover, the resulting charged species are thermodynamically very stable. The interesting properties of the TTF-based compounds are usually related to changes on the oxidation state, and these changes bring about remarkable modifications on both the molecular and the electronic structure. As a consequence,

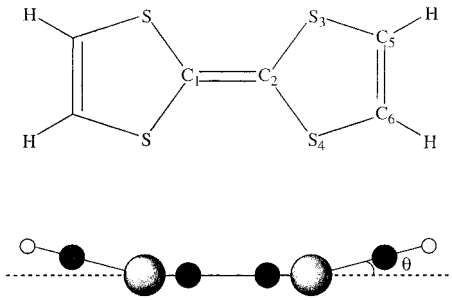

Figure 1. Structure and atom labeling for tetrathiafulvalene.

analysis of the corresponding equilibrium geometry and UV−vis spectrum has become the most extended procedure for determining the oxidation state of the TTF moiety in the system. A theoretical research of the changes occurring in the two properties upon oxidation of neutral TTF to its radical cation has been the main objective of the present contribution. Geometry optimization of both species, as well as calculations of the low-lying excited electronic states, have been undertaken by means of using ab initio techniques.

Special attention has been paid here to the theoretical analysis of the absorption spectra. The excited states of both systems have been calculated within the framework of the multiconfigurational second-order perturbation theory (CASPT2). The successful performance of this approach in computing spectroscopic properties is well established, and the method has shown to yield reliable predictions and interpretations of the electronic spectra of organic molecules in numerous applications.[16−18] The UV−vis spectroelectrochemistry technique, where the evolution of the optical spectrum is measured with respect to the applied potential, has become one of the most powerful tools for the characterization of TTF derivatives. Development of the spectral features of the neutral or the cationic TTF forms makes possible the identification of the oxidation state of the TTF subunit and, therefore, the understanding of the redox role of the system.[19]

* To whom correspondence should be addressed.

10.1021/jp013634g CCC: $22.00
Published on Web 12/28/2001

Hence, the absorption spectrum is actually used as a fingerprint for a given oxidation state. The strategy takes advantage of the decisive differences observed between the UV−vis spectra of the neutral TTF molecule and its charged species, being the spectra for both systems well-known from an experimental point of view. However, only a few theoretical studies, mostly employing semiempirical methods, have tried to throw some light into the interpretation of the recorded spectral features.[20−26] Even though they have provided useful information, several bands of the spectra have not been unambiguously assigned and a number of open questions are still under debate. The current ab initio study is aimed at clarifying these aspects and at giving a full interpretation of the electronic spectra of TTF and TTF^+.

2. Methods and Computational Details

The ground-state geometries of TTF and TTF^+ have been optimized at the CASSCF level, including the π and π^* valence molecular orbitals (MOs) in the active space (π-CASSCF), that is, 10 active MOs and 14(TTF)/13(TTF^+) active electrons. Generally contracted basis sets of Atomic Natural Orbital (ANO) type have been used, obtained from S(17s12p5d)/C(14s9p4d)/H(8s) primitive sets with the contraction scheme S[4s3pld]/C[3s2p1d]/H[2s].[27,28] The basis set has been shown in previous studies to be flexible enough for a proper description of ground and valence excited states.[29−31] For the neutral system, the gas-phase molecular structure determined by electron diffraction exhibited a nonplanar boatlike (C_{2v}) conformation.[32] Nevertheless, theoretical calculations have pointed out that the energy profile for the planarization is very flat and that the floppy inversion motion between the C_{2v} arrangement and the D_{2h} planar structure has an extremely small energy barrier.[33−37] Therefore, geometry optimizations have been performed within D_{2h} and C_{2v} symmetries. Previous calculations have also shown that the planar D_{2h} structure is a first-order saddle point with only one imaginary frequency,[35,37] and no minima corresponding to a chairlike C_{2h} conformation has been found.[35,36] In the cationic species, previous theoretical calculations led to planar D_{2h} equilibrium conformations.[34−37] As far as we know, no geometrical experimental data determined on gas phase are available, although a planar D_{2h} structure has also been suggested on the basis of X-ray crystallographic measurements.[38,39] Consequently, the geometry optimization of the cation has been carried out within D_{2h} symmetry.

For the computation of the vertical excitation energies, the basis set was supplemented with a set of specifically designed 1s1p1d Rydberg-type functions contracted from a set of 8s8p8d primitives, placed at the center of the molecule, according to the procedure explained elsewhere.[16] Such an enlargment of the basis set is required for the adequate representation of the Rydberg excited states. Thus, a total number of 173 basis functions were used in the calculation of the electronic states. The D_{2h} optimized geometries have been employed for the computation of the vertical excitation energies, placing the molecule in the *yz* plane with the long molecular axis along the *z* axis. According to the theoretical calculations, the most stable conformation for the neutral system does not correspond to a D_{2h} planar arrangement but to a slightly distorted C_{2v} structure, as it will be discussed in the next section. Nevertheless, from a series of test calculations carried out to check the influence of the geometry in the calculated transition energies, we can conclude that similar computed spectra are obtained for the D_{2h} and C_{2v} structures of TTF. Thus, a D_{2h} planar geometry was chosen for the study of the neutral molecule.

The vertical excitation energies have been computed by means of the multistate (MS) extension of the CASPT2 approach. In the CASPT2 method,[40−42] the first-order wave function and the second-order energy in a full CI space are calculated using the CASSCF wave function as reference. This reference includes all strongly interacting configurations, and the remaining (dynamic) correlation effects are taken into account in a second-order perturbation treatment. In the MS−CASPT2 procedure,[43] an effective Hamiltonian, including a number of states, is solved. The diagonal elements correspond to the CASPT2 energies and the off-diagonal elements introduce the coupling to second order in the dynamic correlation energy. Thus, the considered states are allowed to interact under the influence of the dynamic correlation. This extension has been shown to provide accurate excitation energies and an adequate description of the main spectral features in a number of previous studies.[44−48]

The π valence active space is the natural choice to perform the calculations. It comprises the 10 valence π-orbitals together with 14 active electrons for TTF and 13 for TTF^+. Besides $\pi\pi^*$ excitations, low-lying states described by $\pi\sigma^*$ promotions have also been considered. Accordingly, the active space had to be enlarged when computing such states by including the required σ^* orbitals. Apart from valence states, the lowest members of the Rydberg series converging to the first ionization potential have also been taken into account for the neutral system, extending the active space to include the 3s, 3p, and 3d orbitals. The simultaneous inclusion of nine one-electron functions would yield an excessive number of active orbitals. Thus, the enlargement was carried out by adding selected sets of Rydberg orbitals to the π-valence space, which means including only those Rydberg orbitals required to compute the Rydberg states of a given symmetry, because the remaining Rydberg orbitals act mainly as virtual orbitals. The calculation of the valence singlet states has been performed simultaneously with the Rydberg states. The computed excitation energies have been checked with respect to further enlargements of the active space. From such an analysis, additional orbitals had to be incorporated into the active space in some particular cases. The final active spaces employed for the computation of the excited states of TTF and TTF^+, the number of configuration state functions (CSFs), and the number of state-averaged CASSCF roots are compiled in Table 1. The carbon and sulfur 1s electrons were kept frozen in the form determined by the ground-state SCF wave function, and they were not included in the second-order correlation treatment.

The linear combination of the CAS states produced by the MS−CASPT2 computation has been named Perturbatively Modified CAS (PMCAS) CI wave function.[43] The oscillator strengths were computed using PMCAS-CI transition dipole moments according to the CAS state interaction (CASSI) protocol.[49,50] Energy differences corrected by MS−CASPT2 correlation energies have been utilized in the oscillator strength formula. All calculations have been performed with the MOLCAS-4 program package.[51]

3. Results and Discussion

3.1 Ground-State Optimized Geometry. The optimized geometrical parameters computed at the π-CASSCF level for the ground state of tetrathiafulvalene and its radical cation are listed in Table 2. Available experimental data are also included for the sake of comparison.

The equilibrium structure calculated for neutral TTF corresponds to a C_{2v} conformation. The central $(S)_2C{=}C(S)_2$ group is nearly planar and the dithiole rings are slightly folded along the S···S axes, with the two HC═CH groups lying on the same side of the molecular plane, in a boatlike arrangement (see

TABLE 1: CASSCF Wave Functions Employed to Compute the Electronic States of Tetrathiafulvalene (TTF) and Its Radical Cation (TTF^+)

active space[a]	states	config.[b]	N_{states}[c]
	TTF		
14/04020302	^1A_g	8290	2
14/43020302	$^1B_{3u}$	344880	4
	$^3B_{3u}$	626360	4
14/03030302	$^1B_{2u}$	8130	2
	$^3B_{2u}$	12730	2
14/03220302	$^1B_{1g}$	20820	2
14/13122302	$^1B_{2g}$	344620	2
14/03020302	$^1B_{3g}$	1220	1
	$^3B_{3g}$	1740	1
14/03020402	$^1B_{1u}$	8140	2
	$^3B_{1u}$	12720	2
14/03020312	^1A_u	3470	1
	TTF^+		
13/04020302	$^2B_{3u}$	19100	3
13/03020302	$^2B_{2g}$	3470	2
13/23020302	^2A_g	41972	2
13/03030302	$^2B_{1g}$	19070	4
13/03020302	^2A_u	3460	2
13/13021302	$^2B_{1u}$	41922	1
13/03120302	$^2B_{2u}$	8690	1

[a] Number of active electrons/number of active orbitals belonging to the irreducible representations a_g, b_{3u}, b_{2u}, b_{1g}, b_{1u}, b_{2g}, b_{3g}, and a_u, respectively, of the D_{2h} point group. [b] Number of Configuration State Functions (CSFs). [c] Number of state-averaged CASSCF roots.

TABLE 2: Geometrical Parameters for the Ground State of Tetrathiafulvalene (TTF) and Its Radical Cation (TTF^+) Optimized at the π-CASSCF Level

	TTF			TTF^+	
parameter[a]	calc. (C_{2v})	calc. (D_{2h})	exp.[b]	calc.	exp.[c]
$r(C_1-C_2)$	1.345	1.346	1.358 ± 0.005	1.401	1.38−1.41
$r(C_2-S_3)$	1.780	1.780	1.767 ± 0.004	1.726	1.71−1.72
$r(S_3-C_5)$	1.762	1.761	1.753 ± 0.004	1.738	1.71−1.73
$r(C_5-C_6)$	1.336	1.337	1.348 ± 0.004	1.344	1.30−1.35
r(C−H)	1.082	1.082	1.105 ± 0.008	1.082	0.8−1.1
$\angle(S_3-C_2-S_4)$	113.9	114.1	114.2 ± 0.6	115.1	115−116
$\angle(C_2-S_3-C_5)$	94.7	95.0	94.5 ± 0.6	95.6	94−96
$\angle(S_3-C_5-C_6)$	117.9	118.0	117.6 ± 0.3	116.8	117−118
$\angle(C_5-C_6-H)$	124.5	124.5	123.5 ± 1.1	125.3	
θ	10.3	0	13.5 ± 4.2		

[a] Bond distances in Å and angles in degrees. For atom labeling see Figure 1. [b] Determined from the gas-phase electron diffraction measurements.[32] [c] Determined from X-ray crystallographic measurements.[38,39,72,73]

Figure 1). The degree of folding is described in terms of the dihedral angle between the $S_3C_2S_4$ and $S_3C_5C_6S_4$ planes (θ). A similar nonplanar conformation is also proposed experimentally because it gives the best fit to the observed intensity patterns in the gas-phase electron diffraction measurements.[32] The CASSCF geometrical parameters compare well with the so-derived values. The computed folding angle is found to be 10.3° and lies within the interval determined experimentally, $13.5 \pm 4.2°$.[32]

An additional optimization was carried out by forcing the molecule to be planar. Knowledge of the main features of the boat-planar distortion is especially relevant because the motion has been suggested to play a crucial role in the mechanism of superconductivity in organic conductors involving TTF derivatives as donor groups. Indeed, the electron−phonon coupling resulting from the electron transfer between neutral and charged-donor forms coupled with the soft conformational motions (boat-planar) associated with the transfer has been proposed to be responsible for the superconductivity in this type of molecular organic conductors.[52] When D_{2h} symmetry constraints (planar arrangement) are imposed during the geometry optimization, the bond distances and angles remain almost unaltered with respect to the values obtained for the C_{2v} equilibrium structure (cf. Table 2). At the CASSCF level, the planar conformation is computed to lie only 0.03 kcal/mol above the boatlike structure. When dynamical correlation effects are included by means of the CASPT2 approach, using the CASSCF optimized geometries, the energy difference hardly increases to 0.14 kcal/mol. Calculations previously reported estimated that the zero-point vibrational energy corrections can additionally decrease the energy difference by about 0.04 kcal/mol.[33] Accordingly, the planarization motion is predicted to have no significant barrier.

The present results confirm the conclusions reported in previous theoretical studies concerning the highly flexible structure of TTF,[33−37] which is reflected on the very different conformations that the TTF skeleton has in the solid state. For instance, X-ray data reveal that TTF has nearly planar conformations in the two polymorphic structures found in crystal.[53−55] On the other hand, TTF derivatives with the TTF moiety severely bent have also been synthesized.[56]

Oxidation of tetrathiafulvalene yields, as expected, significant changes in the geometry. On the basis of theoretical calculations, the TTF^+ radical cation has been predicted to have a D_{2h} planar equilibrium structure.[34−37] An identical conclusion has been reached from the available experimental data, obtained from X-ray crystallographic measurements.[38,39] Planarization of the system upon the loss of an electron has a crucial impact for the understanding of the superconductivity mechanism taking place in the above-mentioned related materials.[52] The geometrical parameters obtained for the ground state of TTF^+ at the π-CASSCF level of calculation are summarized in Table 2. The optimized bond lengths and bond angles of the D_{2h} equilibrium structure are in agreement with the available experimental data. In some cases, the bond distances computed for the cation differ substantially from those obtained for the neutral TTF. The interannular C═C bond (C_1═C_2) is elongated by 0.055 Å upon ionization. In contrast, the S−C bonds are shortened by 0.054 (S_3–C_2) and 0.023 Å (S_3–C_5). The outer C═C bonds (C_5═C_6) are little affected; they are lengthened by 0.007 Å. The modifications can be rationalized on the basis of a simple MO model. The ground state of TTF^+ is mainly described by the singly excited configuration built by removing an electron from the highest occupied MO (HOMO) of the principal configuration of the ground state of TTF. The HOMO exhibits bonding character over the C═C bonds and antibonding character over the S−C bonds. Consequently, upon electron detachment, the bond distances are expected to be increased in the former and decreased in the latter. The most severe changes in the geometrical parameters involve the central $(S)_2C$═$C(S)_2$ group. The optimized C_1–C_2 distance, 1.401 Å, is between the values expected for standard double and single carbon−carbon bond lengths, reflecting the occurrence of that partial transformation. Furthermore, the structural modifications give rise to a partial gain of aromaticity. The S−C bond distances become shorter and closer to the value found in a typical aromatic ring such as thiophene (1.714 Å[57]). Contribution from 6π-electron heteroaromaticity of the 1,3-dithiolium cation is responsible for the large thermodynamic stability of TTF^+, one of the key properties that make TTF such an interesting building block for new materials.[12]

3.2 Vertical Excited States of TTF. The results obtained for the electronic states of TTF, computed at the D_{2h} optimized geometry, are listed in Table 3. The first column identifies the

TABLE 3: Vertical Excitation Energies and Oscillator Strengths for the Electronic States of TTF

state	excitation energies (eV) PMCAS-CI	MS−CASPT2	exp.	osc. str.
Singlet States				
1^1A_g				
1^1B_{3u} ($\pi\sigma^*$)	4.81	2.08		<0.001
1^1B_{2u} ($\pi\pi^*$)	5.87	3.05	3.37[a], 3.35[b]	0.062
1^1B_{1g} ($\pi\sigma^*$)	5.83	3.31		forbidden
1^1B_{2g} ($\pi\sigma^*$)	5.66	3.41		forbidden
1^1B_{3g} ($\pi\pi^*$)	6.01	3.44		forbidden
2^1B_{3u} ($H\rightarrow$3s)	4.92	3.63		0.022
2^1B_{2g} ($H\rightarrow$3p$_z$)	5.50	3.80		forbidden
1^1B_{1u} ($\pi\pi^*$)	6.40	4.01	4.09[c]	0.376
2^1B_{1g} ($H\rightarrow$3p$_y$)	5.16	4.29		forbidden
2^1A_g ($H\rightarrow$3p$_x$)	5.16	4.40		forbidden
3^1B_{3u} ($H\rightarrow$3d$_{x^2-y^2}$)	5.36	4.62		0.005
1^1A_u ($H\rightarrow$3d$_{yz}$)	5.18	4.65		forbidden
2^1B_{1u} ($H\rightarrow$3d$_{xz}$)	5.75	4.73		0.012
4^1B_{3u} ($H\rightarrow$3d$_{z^2}$)	5.47	4.78		<0.001
2^1B_{2u} ($H\rightarrow$3d$_{xy}$)	5.74	4.84		0.014
Triplet States				
1^3B_{3u} ($\pi\sigma^*$)	4.58	1.92		
1^3B_{1u} ($\pi\pi^*$)	3.78	2.76	2.76[a], 2.72[b]	
1^3B_{2u} ($\pi\pi^*$)	4.21	2.89		
1^3B_{3g} ($\pi\pi^*$)	4.09	3.11		

[a] In cyclohexane[21] and in hexane.[60] [b] In hexane.[61] [c] Two close-lying peaks have been detected. The peak with the largest extinction coefficient is located at 4.09 eV and the second peak has been found at 3.91−3.92 eV.[21,60,61]

different excited states of TTF. The nature of the wave functions is shortly described within parentheses. For valence states, the $\pi\pi^*$ or $\pi\sigma^*$ character is indicated. In the Rydberg states, the two orbitals involved in the corresponding one-electron promotion are given. The second and third columns report the vertical excitation energies computed at the PMCAS-CI and MS−CASPT2 levels, respectively. The available experimental values measured in nonpolar solvents are listed in column four. Column five collects the calculated oscillator strengths.

The PMCAS-CI wave functions calculated for the valence states of TTF are summarized in Table 4. The configurations with coefficients larger than 0.05 have been classified into three groups, according to the number of excitations with respect to the main configuration of the ground state. The number of configurations and the weights for each group are reported on the left-hand side of the table. The principal configurations are listed, together with their weights, on the right side. To simplify the notation, they are described as electronic excitations from the principal configuration of the ground state.

A preliminary analysis of the molecular orbitals distribution can be helpful to understand the most important features of the calculated wave functions. The orbital energy levels close to the HOMO and the lowest unoccupied MO (LUMO) calculated at the SCF level are depicted in Figure 2. The five highest occupied MOs are computed to be of π nature. The electronic spectrum of TTF is determined to a large extent by the HOMO, spaced from the remaining occupied orbitals more than 2 eV apart. The calculations place the seven lowest unoccupied molecular orbitals within a narrow energy range. They correspond to the three valence π^* orbitals and four σ^* orbitals. The LUMO exhibits σ^* character.

3.2.1 Spectrum Region: 1.9−3.0 eV. According to the MS−CASPT2 results compiled in Table 3, the most intense transitions of the electronic spectrum of TTF involve singlet excited states of $\pi\pi^*$ character. The excited states are computed to lie more than 3 eV above the ground state. In the UV−vis absorption spectra of the system recorded in different solvents, a very weak band located around 2.7−2.8 eV is, however, observed.[20,21,58−62] The interpretation of such an absorption has become a rather controversial issue, and four different assignments have been proposed. Coffen et al.[21] carried out extended Hückel (EH) calculations and assigned the band to the lowest allowed transition, corresponding to the excitation from the HOMO (a b_{3u} π orbital) to the LUMO (an a_g σ orbital). The $\pi-\sigma^*$ character of the transition matches with the low intensity

TABLE 4: PMCAS-CI Wave Functions for Tetrathiafulvalene: Number (Weights) of Singly (S), Doubly (D), and Triply (T) Excited Configurations[a] with Coefficients Larger than 0.05, Principal Configurations and Weights

state	no. conf. (weight) S	D	T	principal configurations	%
1^1A_g		13(11%)		$(2b_{3u})^2(2b_{2g})^2(3b_{3u})^2(2b_{1g})^2$-$(2a_u)^2(3b_{2g})^2(4b_{3u})^2$	88
1^1B_{3u}	3(89%)		8(4%)	$(4b_{3u}) \rightarrow (13a_g)$	63
				$(4b_{3u}) \rightarrow (14a_g)$	19
				$(4b_{3u}) \rightarrow (15a_g)$	7
1^1B_{2u}	3(85%)	8(7%)	5(2%)	$(4b_{3u}) \rightarrow (3b_{1g})$	84
1^1B_{1g}	2(89%)		10(5%)	$(4b_{3u}) \rightarrow (10b_{2u})$	63
				$(4b_{3u}) \rightarrow (11b_{2u})$	26
1^1B_{2g}	5(80%)	4(6%)	4(1%)	$(4b_{3u}) \rightarrow (12b_{1u})$	53
				$(3b_{2g}) \rightarrow (13a_g)$	22
1^1B_{3g}	3(82%)	8(11%)	5(2%)	$(4b_{3u}) \rightarrow (3a_u)$	78
				$(4b_{3u})^2 \rightarrow (3b_{1g})(4b_{2g})$	7
1^1B_{1u}	2(88%)	3(3%)	8(5%)	$(4b_{3u}) \rightarrow (4b_{2g})$	86
1^3B_{3u}	4(89%)		7(4%)	$(4b_{3u}) \rightarrow (13a_g)$	69
				$(4b_{3u}) \rightarrow (14a_g)$	19
1^3B_{1u}	4(91%)	2(1%)	7(5%)	$(4b_{3u}) \rightarrow (4b_{2g})$	87
1^3B_{2u}	3(90%)		8(5%)	$(4b_{3u}) \rightarrow (3b_{1g})$	48
				$(3b_{2g}) \rightarrow (3a_u)$	35
				$(3b_{3u}) \rightarrow (3b_{1g})$	8
1^3B_{3g}	2(91%)		5(7%)	$(4b_{3u}) \rightarrow (3a_u)$	50
				$(3b_{2g}) \rightarrow (3b_{1g})$	41

[a] With respect to the ground-state principal configuration.

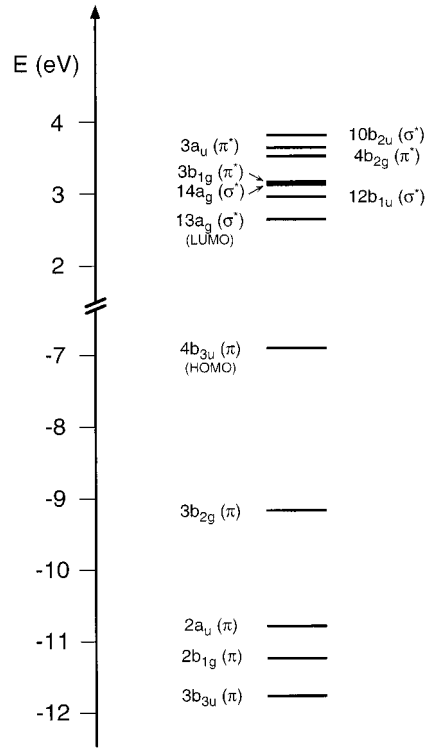

Figure 2. Schematic diagram showing the molecular orbital distribution near the HOMO−LUMO gap of tetrathiafulvalene.

observed for the absorption. However, this weak band was attributed to an $n-\pi^*$ transition by Zahradník et al.[20] in another semiempirical study. Gleiter et al.[63] measured the electronic spectrum of TTF in stretched polyethylene film by using light polarized along the two molecular axes, detecting a parallel and a perpendicular component for the band. It was explained by assigning the weak feature to a forbidden $\pi\rightarrow\pi^*$ transition involving a B_{3g} excited state, which became allowed by coupling with b_{1u} and b_{2u} vibrations.[63,64] Bennett and Herman[22] offered a different assignment on the basis of the results obtained from Xα calculations. They proposed that the feature was due in part to two singlet−triplet $\pi\pi^*$ transitions. The excitations involved $^3B_{1u}$ and $^3B_{2u}$ states, the respective transitions having long-axis and short-axis polarization. Spin−orbit interaction associated with the sulfur atoms was suggested as the responsible mechanism for the observed intensity. Nevertheless, the authors did not exclude that the $\pi-\sigma^*$ HOMO→LUMO transition, polarized along the symmetry axis perpendicular to the molecular plane, also played a role if some of the TTF molecules were slightly misaligned. Indeed, such a $\pi-\sigma^*$ excitation was chosen as the most plausible candidate for the assignment of the lowest-energy absorption in subsequent theoretical studies.[24,25] To check the validity of all these hypotheses and elucidate the nature of the band, the current theoretical study was extended to the lowest-lying $\pi-\sigma^*$ singlet and $\pi-\pi^*$ triplet states, and the results are also included in Tables 3 and 4.

The SCF MOs distribution calculated for TTF has no *n* orbital among the highest occupied molecular orbitals (see Figure 2). Thus, no $n-\pi^*$ transition is expected to be found in the energy region where the onset of absorption is recorded. Indeed, test calculations revealed that excited states of this type lie in a much higher energy region. Consequently, this assignment can be ruled out. The possibility that a $\pi\pi^*$ forbidden transition involving a B_{3g} excited state is responsible for the 2.7−2.8 eV weak band can also be discarded, since the excitation energy computed at the MS−CASPT2 level for the $1^1A_g\rightarrow1^1B_{3g}$ transition, 3.44 eV, is about 0.7 eV higher than the experimental value (see Table 3). As regards the assignment to a $\pi-\sigma^*$ excitation, it represents a good candidate in view of the fact that the lowest unoccupied MOs are σ^* orbitals. As shown in Table 3, the calculations predict that the allowed HOMO→LUMO $\pi-\sigma^*$ 1^1B_{3u} state is the lowest-lying singlet excited state of TTF. It is computed to lie 2.08 eV above the ground state at the MS−CASPT2 level, with a negligible related oscillator strength. Therefore, it seems rather unlikely that the $1^1A_g\rightarrow1^1B_{3u}$ transition can be responsible for such a feature. To check whether another $\pi-\sigma^*$ excitation might be involved, higher-lying excited states of this type were calculated. In order of increasing energy, the next $\pi-\sigma^*$ singlet states were computed to be of B_{1g} and B_{2g} symmetry. The corresponding transitions are optically forbidden, and the computed vertical excitation energies at the MS−CASPT2 level are 3.31 and 3.41 eV, respectively, that is, more than 0.5 eV higher than the experimental data. Consequently, the assignment of the lowest-energy band to a $\pi-\sigma^*$ transition can also be ruled out.

As far as the low-lying triplet states are concerned, the MS−CASPT2 calculations place three $\pi\pi^*$ triplet states very close in energy. The states are of B_{1u}, B_{2u}, and B_{3g} symmetry and the corresponding excitation energies are computed to be 2.76, 2.89, and 3.11 eV, respectively. The most important configuration of their wave functions represents a one-electron promotion from the HOMO to one of the three valence π^* MOs. Nevertheless, only in the $^3B_{1u}$ state is the wave function clearly dominated by a single configuration. The relative energy predicted for the $^3B_{1u}$ and $^3B_{2u}$ states coincides with the energy interval in the visible region where the weak band was observed. Transitions to the $^3B_{1u}$ and $^3B_{2u}$ states are respectively polarized along the long and short molecular axes, in agreement with the two components observed experimentally for that band when polarized light is used.[63] In view of the results obtained here, one can conclude that the lowest-energy band of the electronic spectrum of TTF is due to two transitions involving the 1^3B_{1u} and 1^3B_{2u} electronic states. The results give support to the assignment proposed by Bennett and Herman, who rationalized the experimental findings on the basis of such triplet states, attributing the observed intensity in the absorption spectrum to spin−orbit effects.[22]

3.2.2 Spectrum Region: 3.0−4.9 eV. The calculations carried out in the present work place three valence $\pi\pi^*$ electronic states in the energy range 3.0−4.1 eV. They are the 1^1B_{2u}, 1^1B_{3g}, and 1^1B_{1u} states, with excitation energies of 3.05, 3.44, and 4.01 eV, respectively. Transition to the 1^1B_{3g} state is dipole forbidden and the other two are allowed. Whereas that involving the 1^1B_{2u} state shows a small calculated oscillator strength, the corresponding value for the $1^1A_g\rightarrow1^1B_{1u}$ transition is relatively large (see Table 3). The wave functions are dominated by a one-electron promotion, from the HOMO to one of the three valence π^* MOs available.

The electronic absorption spectrum of TTF presents, in this region, strong absorption in the energy interval 3.9−4.3 eV and a weak band around 3.3−3.5 eV as a shoulder on the tail of the former.[20,21,58,60−63,65] The strong feature exhibits two close-lying intense peaks. The largest extinction coefficient corresponds to the peak located, in nonpolar solvents, at 4.09 eV, whereas the additional peak occurs at 3.91−3.92 eV and has an absorbance slightly smaller than the former.[21,60,61] According to the MS−CASPT2 results, the only candidate for such an absorption is the $1^1A_g\rightarrow1^1B_{1u}$ transition computed at 4.01 eV. The assignment is in accordance with the long-axis polarization direction determined experimentally for this band,[63] as well as with previous theoretical results.[20−22] However, on the basis of extended Hückel calculations, Coffen et al. suggested that the two peaks detected were due to two different $\pi\pi^*$ electronic transitions, mainly corresponding to HOMO→$3b_{1g}$ and HOMO→$4b_{2g}$ one-electron promotions.[21] The same conclusion was reached by Batsanov et al. from the analysis of their CNDO/S results.[25] The values obtained in the present work do not support this interpretation, since the respective excited states, 1^1B_{2u} and 1^1B_{1u}, differ by more than 0.9 eV from each other. The occurrence of two close features must be probably attributed to the vibrational structure of the band. As regards the shoulder around 3.37 eV, four valence states might be responsible for such a feature, on the basis of the computed excitation energies, namely, 1^1B_{2u}, 1^1B_{1g}, 1^1B_{2g}, and 1^1B_{3g}. However, only the former is dipole allowed. Hence, the weak band is assigned to the $\pi\pi^*$ $1^1A_g\rightarrow1^1B_{2u}$ transition. As mentioned above, it exhibits an oscillator strength considerably smaller than the most intense band, in agreement with experimental evidence. Nevertheless, the predicted excitation energy, 3.05 eV, is somewhat deviated from the experimental value. The assignment proposed also agrees with the short-axis polarized character of the band observed spectroscopically[63] and with those previously reported by Zahradník et al.[20] and Bennett et al.[22] An assignment involving a forbidden $\pi\sigma^*$ transition, as suggested by Coffen et al.,[21] seems to be rather improbable.

Apart from valence transitions, several Rydberg states are computed to lie below 5 eV. The excitation from the HOMO to the 3s orbital gives rise to the lowest-energy member. At the

TABLE 5: Vertical Excitation Energies and Oscillator Strengths for the Electronic States of TTF^+. Experimental Data Are Also Included

	excitation energies (eV)			
state	PMCAS−CI	MS−CASPT2	exp.	osc. str.
1^2B_{3u} (π-hole)				
1^2B_{2g} (π-hole)	2.87	2.22	2.14[a,b]	0.075
1^2A_g (σ-hole)	3.76	2.36		<0.001
1^2B_{1g} (π-hole)	4.13	2.45	2.51[b]	0.003
1^2A_u (π-hole)	3.89	2.97		forbidden
2^2B_{2g} (π-hole)	3.63	3.01	2.90[a], 2.86[b]	0.498
2^2A_u (π-hole)	4.12	3.27		forbidden
1^2B_{1u} (σ-hole)	5.29	3.58		forbidden
2^2B_{1g} (π-hole)	4.44	3.59	3.67[b]	0.191
2^2B_{3u} (π-hole)	4.67	3.82		forbidden
1^2B_{2u} (σ-hole)	5.23	3.83		forbidden

[a] Absorption maximum in a Freon glass.[26] [b] Absorption maximum in acetonitrile.[58]

MS−CASPT2 level, it is placed at 3.63 eV. The electronic transition is allowed, with a computed oscillator strength of 0.02. Unfortunately, as far as we know, no experimental information about Rydberg states is available for TTF. The dipole-forbidden 3p Rydberg states are found in the same region that the intense valence band, between 3.8 and 4.4 eV, and the 3d Rydberg states are predicted to lie in the energy interval 4.6−4.9 eV. Only two states belonging to the 3d set, 2^1B_{1u} and 2^1B_{2u}, have oscillator strengths larger than 0.01.

Inspection of higher-energy roots shows that, in addition to a given number of forbidden states as well as allowed states with small oscillator strengths, two intense $\pi\pi^*$ valence transitions can be predicted around 5.3 eV (MS−CASPT2 results). They involve excited states of B_{1u} and B_{2u} symmetries. Nevertheless, these states have not been included in the tables because higher members of the Rydberg series not considered here are also expected in this energy region.

3.3 Vertical Excited States of TTF^+. Table 5 contains the results obtained for the low-lying doublet states of TTF^+, together with the available experimental data. The first column reports, within parentheses, the character of the orbital where the unpaired electron (and, therefore, the hole) is located. The corresponding wave functions are summarized in Table 6. The optimized geometry of the radical cation, listed in Table 2, has been employed for the calculations.

The ground state of TTF^+ belongs to the $^2B_{3u}$ symmetry. The wave function is dominated by a single configuration built by removing one electron from the $4b_{3u}$ π-orbital (HOMO).

The observed electronic spectrum of TTF^+ has important differences with that of the neutral molecule. Whereas TTF does not absorb in the visible region, with the only exception of the exceedingly small contribution at 2.76 eV, the spectrum of its cation exhibits several significant features below 3.1 eV, including the most intense band. At the MS−CASPT2 level of calculation, the two lowest-lying doublet excited states are predicted to be of B_{2g} and A_g symmetry, placed at 2.22 and 2.36 eV, respectively. The corresponding transitions from the ground state are dipole allowed. The wave functions are dominated in both cases by one configuration, but they are very different in nature (cf. Table 6). In terms of the one-electron levels depicted in Figure 2, the 1^2B_{2g} state is mainly described by the promotion HOMO-1→HOMO, that is, an excitation between π orbitals. However, the transition to the 1^2A_g state involves the HOMO→LUMO excitation, the unpaired electron being promoted from a π to a σ^* orbital.

The visible absorption spectra of this cation recorded in liquid solutions at room temperature are characterized by a band in the yellow region, with a maximum around 2.14 eV.[20,21,58,65−67] The feature has also been detected in the absorption and excitation spectra of TTF^+ generated by irradiation in low-temperature organic glasses.[26] Previous theoretical calculations, employing semiempirical approaches, have provided two different interpretations. According to the PPP calculations reported by Zahradník et al.,[20] the band can be associated with the $1^2B_{3u}\rightarrow1^2B_{2g}$ transition, involving the $3b_{2g}\rightarrow4b_{3u}$ promotion. This transition between π orbitals was also proposed by Zimmer et al. on the basis of their LNDO/S PERTCI results.[26] In contrast, extended Hückel calculations performed by Coffen et al.[21] led these authors to assign the band to the dipole-allowed $1^2B_{3u}\rightarrow1^2A_g$ transition of $\pi-\sigma$ character, involving the HOMO→LUMO promotion. Identical lowest-energy allowed excitation was found by Batra et al.[23] in their Xα study.

TABLE 6: PMCAS−CI Wave Functions for TTF^+: Number (Weights) of Singly (S), Doubly (D), and Triply (T) Excited Configurations[a] with Coefficients Larger than 0.05, Principal Configurations and Weights

	no. conf. (weight)				
state	S	D	T	principal configurations	%[b]
1^2B_{3u}		12(7%)		$(2b_{3u})^2(2b_{2g})^2(3b_{3u})^2(2b_{1g})^2$-$(2a_u)^2(3b_{2g})^2(4b_{3u})^1$	89 (89)
1^2B_{2g}	5(87%)	4(3%)	4(2%)	$(3b_{2g})\rightarrow(4b_{3u})$	73 (83)
				$(4b_{3u})\rightarrow(4b_{2g})$	12 (4)
1^2A_g	2(85%)	3(2%)	7(3%)	$(4b_{3u})\rightarrow(13a_g)$	73 (71)
				$(4b_{3u})\rightarrow(14a_g)$	13 (13)
1^2B_{1g}	8(84%)	11(7%)	2(1%)	$(4b_{3u})\rightarrow(3b_{1g})$	73 (32)
				$(3b_{2g})\rightarrow(3a_u)$	5 (4)
				$(2b_{1g})\rightarrow(4b_{3u})$	3 (47)
1^2A_u	5(85%)	12(6%)	7(4%)	$(2a_u)\rightarrow(4b_{3u})$	80 (81)
2^2B_{2g}	4(87%)	6(3%)	8(3%)	$(4b_{3u})\rightarrow(4b_{2g})$	72 (79)
				$(3b_{2g})\rightarrow(4b_{3u})$	11 (3)
2^2A_u	6(85%)	4(5%)	5(3%)	$(4b_{3u})\rightarrow(3a_u)$	49 (45)
				$(3b_{2g})\rightarrow(3b_{1g})$	28 (30)
				$(3b_{3u})\rightarrow(3a_u)$	5 (6)
1^2B_{1u}	3(84%)	4(3%)	7(2%)	$(4b_{3u})\rightarrow(12b_{1u})$	69 (62)
				$(3b_{2g})\rightarrow(13a_g)$	11 (15)
2^2B_{3u}	10(77%)	11(9%)	3(2%)	$(3b_{3u})\rightarrow(4b_{3u})$	69 (69)
				$(2b_{3u})^2(2b_{2g})^2(3b_{3u})^2(2b_{1g})^2$-$(2a_u)^2(3b_{2g})^2(4b_{3u})^1$	4 (6)
2^2B_{1g}	7(84%)	9(5%)	7(3%)	$(2b_{1g})\rightarrow(4b_{3u})$	76 (35)
				$(4b_{3u})\rightarrow(3b_{1g})$	2 (39)
1^2B_{2u}	1(86%)	6(2%)	7(4%)	$(4b_{3u})\rightarrow(10b_{2u})$	86 (85)

[a] With respect to the ground-state principal configuration. [b] Weights obtained at the optimized planar geometry of neutral TTF are indicated within parentheses.

The results obtained at the MS−CASPT2 level confirm the former interpretation, that is, that involving the 1^2B_{2g} excited state (cf. Table 5). The computed vertical excitation energy for this state (2.22 eV) is closer to the experimental value (2.14 eV) than that corresponding to the 1^2A_g state (2.36 eV). In addition, the transition to the latter is computed to have a negligible oscillator strength, whereas the value turns out to be significant in the case of the B_{2g} state. The band at 2.14 eV is consequently assigned to the $1^2B_{3u}\rightarrow1^2B_{2g}$ electronic transition with long-axis polarization. The conclusion is in agreement with the results obtained in the study of the absorption spectra of single crystals of TTF^+ salts with polarized light.[38,68]

Additional information about the lowest-lying excited state can be found in the emission spectroscopic study carried out by Zimmer et al.[26] Even though liquid solutions of TTF^+ do not show any luminescence, these authors observed the fluorescence of this cation when generated by irradiation in low-temperature organic glasses. The maximum of the fluorescence band was located around 1.68 eV, that is, 0.4−0.5 eV below the lowest-energy absorption band. To get some insights into

the origin of this fluorescence, we carried out a new series of calculations. First, the geometry of the cation in the 1^2B_{2g} excited state was optimized at the π-CASSCF level by restricting the system to be planar. The S[4s3p1d]/C[3s2p1d]/H[2s] basis set was employed. And second, the energy difference between such a state and the 1^2B_{3u} ground state was computed at the MS−CASPT2 level by employing the same basis sets and active spaces as in the calculation of the vertical spectrum. The adiabatic excitation energy (difference between both states at their respective optimized geometries) was computed to be 1.90 eV, and the vertical emission energy (difference between both states at the geometry of the excited state) was estimated to be 1.71 eV, that is, 0.51 eV lower than the vertical excitation energy of this state. Although the constraints imposed in the geometry optimization prevent us from giving a definitive answer, the excellent agreement between the theoretical results and the experimental data, both regarding the energy difference between the states and the shift with respect to the maximum of the absorption band, leads us to tentatively assign the observed fluorescence to the $1^2B_{2g}\rightarrow 1^2B_{3u}$ transition.

The absorption spectrum of TTF^+ in solution displays an additional band at even lower energies when recorded at low temperatures.[66,67] The feature appears with strong intensity in the red region, around 1.73 eV. Absorption at similar energies was also observed in the spectra of solid TTF^+ salts.[38,66−68] From the analysis of the band, it was concluded that the feature cannot be attributed to an intramolecular excitation of TTF^+; instead, it should be associated to an intermolecular charge transfer of $(TTF^+)_2$ dimers. The MS−CASPT2 results indirectly support this interpretation, since no excited state is predicted below 2 eV for the monomeric TTF^+.

At higher frequencies, the visible spectrum of TTF^+ in liquid solution shows a shoulder at about 2.51 eV.[58] This feature can be also seen in the spectra in solid organic media.[26] The MS−CASPT2 calculations place, in this region, only one excited state, 1^2B_{1g} (see Table 5), described by a HOMO$\rightarrow\pi^*$ one-electron promotion. The transition $1^2B_{3u}\rightarrow 1^2B_{1g}$ is dipole allowed and the oscillator strength is computed to be small. Consequently, such an excitation is predicted to account for the shoulder. Our assignment is in accordance with the results of the polarized spectra, where a short-axis polarized character for this feature has been found.[38,68]

As can be seen in Table 5, the theoretical calculations carried out in the present work predict an additional dipole-allowed transition in the visible region. It corresponds to the $1^2B_{3u}\rightarrow 2^2B_{2g}$ transition, with a computed vertical excitation energy of 3.01 eV and the largest oscillator strength of the studied spectrum (0.498). The most important configuration contributing to the wave function of the excited state is a HOMO$\rightarrow\pi^*$ promotion. The theoretical results agree with the available experimental data. The electronic spectra of TTF^+ in liquid solutions, as well as in organic matrixes, show the most intense peak around 2.9 eV,[20,21,26,58,65−67] and it has been determined to be polarized along the long molecular axis.[38,68] According to the computed excitation energies, the 1^2A_u state, placed at 2.97 eV, could also be a plausible candidate for the assignment of such a band. Nevertheless, this hypothesis can be discarded because the transition is dipole forbidden. The feature is thus ascribed to the $1^2B_{3u}\rightarrow 2^2B_{2g}$ excitation. It also corroborates the assignment suggested in previous theoretical studies for this strong absorption.[20,26,68]

Wudl et al.[65] and Hünig et al.[58] observed in the tail of this band a small shoulder around 3.06−3.08 eV. However, no additional information has been reported about such a feature, neither experimental nor theoretical. The calculations presented here predict no allowed transition at energies slightly higher than that of the most intense band. The 2^2A_u state is located 3.27 eV above the ground state, but the corresponding excitation is dipole forbidden.

TABLE 7: MS−CASPT2 Vertical Ionization Energies of TTF

	calculated		experimental[a]	
cationic state	IP(eV)	ΔE(eV)[b]	IP(eV)	ΔE(eV)[b]
1^2B_{3u}	6.07	0.00	6.70	0.00
1^2B_{2g}	7.99	1.92	8.58	1.88
1^2A_g	8.46	2.39		
1^2B_{1g}	8.79	2.72		
1^2A_u	9.03	2.96	9.71	3.01
2^2B_{1g}	9.14	3.07	10.09	3.39
1^2B_{1u}	9.33	3.26		
2^2B_{2g}	9.46	3.39		
2^2A_u	9.53	3.46		
1^2B_{2u}	9.58	3.51		
2^2B_{3u}	9.73	3.66	10.50	3.80

[a] Data from the gas-phase HeI photoelectron spectrum.[70] [b] Energy difference with respect to the ground state of the cation.

In the near UV region up to 4 eV, the MS−CASPT2 calculations predict the occurrence of several electronic transitions (cf. Table 5), although only that computed at 3.59 eV, $1^2B_{3u}\rightarrow 2^2B_{1g}$, is dipole allowed. It is mainly described by the HOMO-3→HOMO one-electron promotion and is predicted to be intense. Such a description is in agreement with the available experimental data. The absorption spectra have in this region an intense band with a maximum at about 3.6−3.7 eV,[58,65,66] which can be attributed to the $1^2B_{3u}\rightarrow 2^2B_{1g}$ transition. Notice that other close-lying excited states involve dipole-forbidden electronic transitions. The assignment is in accordance with the short-axis polarized character of the band reported in previous studies.[38,68] It also agrees with that suggested on the basis of PPP calculations,[20,68] although the corresponding excitation energy deviated by more than 0.7 eV from the experimental value.

3.4 Excited States of TTF^+ at the Ground-State Geometry of TTF. The gas-phase photoelectron spectra of TTF have also provided interesting information about the position and the nature of the excited states of TTF^+.[63,69,70] To obtain theoretical results directly comparable to the experimental data, the low-lying excited states of TTF^+ were recalculated at the optimized geometry of neutral TTF and, subsequently, the vertical ionization energies were computed. The MS−CASPT2 results, together with the data determined experimentally, are collected in Table 7. The weights of the main configurations contributing to the corresponding wave functions are indicated in the last column of Table 6 within parentheses.

As expected, the lowest-energy ionization leads to the 1^2B_{3u} ground state of the cation. The vertical and adiabatic ionization potentials have been computed to be 6.07 and 5.88 eV, respectively. The vertical value differs from the first potential measured (6.70 eV).[70] Test calculations reveal that the use of the C_{2v} optimized geometry of TTF instead of the planar conformation, or the improvement of the basis set, does not yield a noticeable increase of the computed value. Therefore, such a discrepancy should be probably attributed to the computational method. In this sense, it is pertinent to recall that an underestimation of about 0.4 eV on the first ionization potential has been previously found for other sulfur-containing molecules, like bithiophene and terthiophene, at a similar level of calculation.[31] The source of the underestimation is not clear at present. Incidentally, the deviation is smaller in the case of

similar species without sulfur atoms, like biphenyl (0.20 eV).[71] Nevertheless, deviations between the absolute values of the ionization energies determined by the different experimental groups have also been reported, though the relative spacings of the peaks are in reasonable agreement.[63,69,70] Hence, such spacings have been also included in Table 7 and, as can be seen, most of the MS−CASPT2 results are in reasonable accordance with the experimental values.

The second lowest-lying electronic state of TTF^+ turns out to be 1^2B_{2g} and is located 1.92 eV above the ground state of the cation. The ionization accounts for the second peak of the photoelectron spectrum of TTF, recorded 1.88 eV above the lowest-energy feature. Our assignment is in agreement with that proposed in previous theoretical studies, by using the Koopmans' theorem.[22,24,63,64,69,70] The 1^2A_g state is computed to be the third lowest-lying state, placed 2.39 eV above the ground state. It represents a non-Koopmans state, since its main configuration corresponds to the ionization from the HOMO plus a HOMO→σ^* one-electron promotion, and it is expected to appear as a low-intensity shake-up satellite band in the photoelectron spectrum.

The assignment of the peaks observed within the energy interval 3−4 eV above the lowest feature has given rise to important controversies. The photoelectron spectrum contains three peaks in this region, located at 3.01, 3.39, and 3.80 eV (cf. Table 7). The first attempts to assign them were reported by Gleiter et al.,[63] who performed PPP and extended Hückel calculations and applied the Koopmans' theorem. However, the results obtained with both approaches were completely different and no definitive assignment was suggested. Whereas the PPP calculations attributed the peaks to ionizations from molecular orbitals of a_u, b_{1g}, and b_{3u} symmetries, in order of increasing energy, the corresponding ordering obtained with the EH method was b_{3u}, a_u, and b_{1g}. The latter found additional support in the semiempirical calculations performed by Berlinsky et al.[69] at the EH level, as well as in those carried out by Bennett and Herman[22] with the Xα procedure. In contrast, the Hartree−Fock−Slater calculations done by Trsic and Laidlaw[24] were in line with the former interpretation, as well as the CNDO/2 results reported by Berlinsky et al.[69] In light of the results obtained at the MS−CASPT2 level, the assignment suggested on the basis of EH calculations (b_{3u}, a_u, and b_{1g}) can be ruled out. The 2^2B_{3u} state lies at 3.66 eV relative to the ground state and, thus, it cannot be responsible for the peak found at 3.01 eV. Instead, the 2^2B_{3u} state can be assigned to the feature observed at 3.8 eV. The assignment of the 3.8 eV peak to an electronic state representing an ionization from a b_{3g} σ orbital, which has been also previously suggested,[64] can be ruled out, since the state is computed to lie in a higher-energy interval.

The assignment of the features at 3.01 and 3.39 eV is, however, far from being evident. Seven electronic states are computed to be placed between 2.7 and 3.6 eV. The 1^2B_{1u}, 2^2B_{2g}, 2^2A_u, and 1^2B_{2u} states, located at 3.26, 3.39, 3.46, and 3.51 eV, respectively, are non-Koopmans states. Their wave functions have not considerably changed when passing from the geometry of the cation to the geometry of the neutral (cf. Table 6) and are dominated by excitations from the HOMO. Therefore, they are not expected to account for the strong peaks observed in the spectrum. The 1^2A_u state is mainly described by a configuration dealing with the ionization from the $2a_u$ orbital (HOMO-2). According to its computed energy with respect to the ground state (2.96 eV), it constitutes a good candidate for the assignment of the third peak (observed at 3.01 eV). This interpretation would be in agreement with the ordering provided by application of the Koopmans' theorem (cf. Figure 2). Nevertheless, two states of B_{1g} symmetry are computed to lie very close in energy; they are located at 2.72 and 3.07 eV. The respective wave functions at the optimized geometry of the cation are clearly dominated by a single configuration; a HOMO→π^* promotion for the 1^2B_{1g} state and a HOMO-3→HOMO in the 2^2B_{1g} state (see Table 6). The latter can be seen as the ionization of TTF by extracting the electron from the HOMO-3. Accordingly, the 2^2B_{1g} state would be expected to account for the fourth peak of the photoelectron spectrum, detected at 3.39 eV relative to the first feature. This interpretation would be in agreement with that provided by the Koopmans' theorem and with that proposed in previous semiempirical studies mentioned above. However, the results obtained employing the geometry of TTF reveal that the wave functions of these states change dramatically when passing from the geometry of the cation to that of the neutral species (cf. Table 6). The wave functions cannot be described by a single configuration any more; they present an unequivocal multiconfigurational nature. The weight of a configuration representing an ionization (such as $2b_{1g}\rightarrow 4b_{3u}$) is very similar to the weight of a configuration representing an ionization from the HOMO plus an excitation to a virtual orbital (such as $4b_{3u}\rightarrow 3b_{2g}$) and both are smaller than 0.5. This mixed character prevents us from giving an unambiguous assignment for these two peaks. Even though the ^2A_u and $^2B_{1g}$ states are predicted to be responsible for such features, the exact ordering and, therefore, the validity of the hypothesis previously suggested on the basis of Koopmans' theorem cannot be established from the present results. Further research is required to elucidate this particular issue.

4. Conclusions

Ab initio CASSCF/MS−CASPT2 calculations have been performed on the low-lying electronic states of tetrathiafulvalene and its radical cation. The ground-state geometry of both species has been optimized at the CASSCF level. A C_{2v} boatlike arrangement is predicted to be the most stable conformation for the neutral molecule. The calculated bond distances and angles are in agreement with the available experimental data. Nevertheless, the energy barrier associated to the planarization motion is exceedingly small. Oxidation of TTF gives rise to important changes on the geometrical parameters. The planar structure obtained from the calculations of the cation shows a more aromatic character, reflected on the enlargement of the interannular C=C bond and the shortening of the S−C bonds.

The theoretical analysis of the vertical excited states of TTF enables the understanding of the main features of its electronic spectrum. The most intense bands recorded correspond to $\pi\pi^*$ excitations. The shoulder at about 3.35 eV has been assigned to the short-axis polarized $1^1A_g\rightarrow 1^1B_{2u}$ transition, whereas the strong absorption around 4.1 eV has been attributed to the long-axis polarized $1^1A_g\rightarrow 1^1B_{1u}$ excitation. Assignments previously suggested on the basis of semiempirical calculations, such as a $\pi\sigma^*$ transition for the former or two different $\pi\pi^*$ promotions for the latter can be discarded. The weak absorption detected in the visible region has been attributed to two singlet−triplet $\pi\pi^*$ transitions involving the $^3B_{1u}$ and $^3B_{2u}$ electronic states, spin−orbit effects being responsible for the observed intensity. Other assignments previously reported, such as $n\pi^*$, $\pi\sigma^*$, or forbidden $\pi\pi^*$ singlet−singlet excitations, can be ruled out. The lowest members of the Rydberg series converging to the first ionization potential have been predicted to lie between 3.6 and 4.9 eV above the ground state.

The calculations performed for the electronic states of TTF^+ provide a full interpretation of the available spectroscopic data,

both those derived from experiments with liquid solutions and those obtained from measurements in low-temperature organic glasses. In the visible region, three excited states exhibit a significant computed oscillator strength, namely, 1^2B_{2g}, 1^2B_{1g}, and 2^2B_{2g}. They are respectively responsible for the absorption band observed at 2.14 eV, for the shoulder detected at 2.51 eV, and for the strong peak recorded around 2.9 eV. The 2^2B_{1g} state is predicted to account for the feature observed at 3.67 eV. In all cases, the computed excitation energies agree with the experimental values. Furthermore, the assignments proposed, both for TTF and TTF^+, are in accordance with the results of polarized absorption spectra.

The calculation of the excited states of TTF^+ at the geometry of TTF helped us to rationalize the data obtained from gas-phase photoelectron spectra. The two lowest-energy peaks have been attributed to the 1^2B_{3u} and 1^2B_{2g} states, which can be described as the result of ionizations from the HOMO and HOMO-1, respectively. The peaks observed at 3.01 and 3.39 eV relative to the lowest feature have not been unambiguously assigned at present. Nevertheless, the 1^2A_u state, as well as the mentioned B_{1g} states, are the candidates for such an assignment. The 2^2B_{3u} state, representing the ionization from the HOMO-4, is predicted to account for the band detected 3.80 eV above the first peak. Consequently, the assignment of the peaks found between 3 and 4 eV proposed in some semiempirical studies, involving, in order of increasing energy, ionizations from the $3b_{3u}$, $2a_u$, and $2b_{1g}$ orbitals, can be ruled out.

Acknowledgment. The research reported in this communication has been supported by the projects PB98-1447 and PB97-1377 of Spanish DGES-MEC and by the FEDER project 1FD97-1765-C03-01. The authors thank Dr. L. Serrano-Andrés, Prof. J. Sánchez-Marín, and Dr. A. Sánchez de Merás for fruitful discussions.

References and Notes

(1) Wudl, F.; Wobschall, D.; Hufnagel, E. J. *J. Am. Chem. Soc.* **1972**, *94*, 670.

(2) Ferraris, J.; Cowan, D. O.; Walatka, V.; Perlstein, J. H. *J. Am. Chem. Soc.* **1973**, *95*, 948.

(3) Coleman, L. B.; Cohen, M. J.; Sandman, D. J.; Yamaguchi, F. G.; Garito, A. F.; Heeger, A. J. *Solid State Commun.* **1973**, *12*, 1125.

(4) Jérome, D.; Mazaud, A.; Ribault, M.; Bechgaard, K. *J. Phys. Lett.* **1980**, *41*, L95.

(5) Bechgaard, K.; Jacobsen, C. S.; Mortensen, K.; Pedersen, H. J.; Thorup, N. *Solid State Commun.* **1980**, *33*, 1119.

(6) Parkin, S. S. P.; Engler, E. M.; Schumaker, R. R.; Lagier, R.; Lee, V. Y.; Scott, J. C.; Greene, R. L. *Phys. Rev. Lett.* **1983**, *50*, 270.

(7) Bryce, M. R. *Chem. Soc. Rev.* **1991**, *20*, 355.

(8) Adam, M.; Müllen, K. *Adv. Mater.* **1994**, *6*, 439.

(9) Khodorkovsky, V.; Becker, J. Y. Molecular design of organic conductors. In *Organic Conductors*; Farges, J.-P., Ed.; Marcel Dekker Inc.: New York, 1994; p 75.

(10) Bryce, M. R. *J. Mater. Chem.* **1995**, *5*, 1481.

(11) Jørgensen, T.; Hansen, T. K.; Becher, J. *Chem. Soc. Rev.* **1994**, *23*, 41.

(12) Bryce, M. R. *Adv. Mater.* **1999**, *11*, 11.

(13) Bryce, M. R. *J. Mater. Chem.* **2000**, *10*, 589.

(14) Nielsen, M. B.; Lomholt, C.; Becher, J. *Chem. Soc. Rev.* **2000**, *29*, 153.

(15) Segura, J. L.; Martín, N. *Angew. Chem., Int. Ed. Engl.* **2001**, *40*, 1372.

(16) Roos, B. O.; Fülscher, M. P.; Malmqvist, P.-Å.; Merchán, M.; Serrano-Andrés, L.. Theoretical studies of electronic spectra of organic molecules. In *Quantum Mechanical Electronic Structure Calculations with Chemical Accuracy*; Langhoff, S. R., Ed.; Kluwer Academic Publishers: Dordrecht, The Netherlands, 1995; pp 357−438.

(17) Roos, B. O.; Andersson, K.; Fülscher, M. P.; Malmqvist, P.-Å.; Serrano-Andrés, L.; Pierloot, K.; Merchán, M. Multiconfigurational perturbation theory: Applications in electronic spectroscopy. In *Advances in Chemical Physics*: *New Methods in Computational Quantum Mechanics*; Prigogine, I., Rice, S. A., Eds.; John Wiley & Sons: New York, 1996; Vol. XCIII, pp 219−331.

(18) Merchán, M.; Serrano-Andrés, L.; Fülscher, M. P.; Roos, B. O. Multiconfigurational perturbation theory applied to excited states of organic compounds. In *Recent Advances in Multireference Theory*; Hirao, K., Ed.; World Scientific Publishing Co.: Singapore, 1999; Vol. IV, pp 161−195.

(19) See, for example, Huchet, L.; Akoudad, S.; Levillain, E.; Roncali, J.; Emge, A.; Bäuerle, P. *J. Phys. Chem. B* **1998**, *102*, 7776.

(20) Zahradník, R.; Čársky, P.; Hünig, S.; Kie*β*lich, G.; Scheutzow, D. *Int. J. Sulfur Chem. C* **1971**, *6*, 109.

(21) Coffen, D. L.; Chambers, J. Q.; Williams, D. R.; Garrett, P. E.; Canfield, N. D. *J. Am. Chem. Soc.* **1971**, *93*, 2258.

(22) Bennett, B. I.; Herman, F. *Chem. Phys. Lett.* **1975**, *32*, 334.

(23) Batra, I. P.; Bennett, B. I.; Herman, F. *Phys. Rev. B* **1975**, *11*, 4927.

(24) Trsic, M.; Laidlaw, W. G. *Int. J. Quantum Chem.* **1982**, *21*, 557.

(25) Batsanov, A. S.; Bryce, M. R.; Heaton, J. N.; Moore, A. J.; Skabara, P. J.; Howard, J. A. K.; Ortí, E.; Viruela, P. M.; Viruela, R. *J. Mater. Chem.* **1995**, *5*, 1689.

(26) Zimmer, K.; Gödicke, B.; Hoppmeier, M.; Meyer, H.; Schweig, A. *Chem. Phys.* **1999**, *248*, 263.

(27) Widmark, P.-O.; Malmqvist, P.-Å.; Roos, B. O. *Theor. Chim. Acta* **1990**, *77*, 291.

(28) Widmark, P.-O.; Persson, B. J.; Roos, B. O. *Theor. Chim. Acta* **1991**, *79*, 419.

(29) Rubio, M.; Merchán, M.; Ortí, E.; Roos, B. O. *J. Chem. Phys.* **1995**, *102*, 3580.

(30) Rubio, M.; Merchán, M.; Ortí, E.; Roos, B. O. *Chem. Phys. Lett.* **1996**, *248*, 321.

(31) Rubio, M.; Ortí, E.; Pou-Amérigo, R.; Merchán, M. *J. Phys. Chem. A* **2001**, *105*, 9788.

(32) Hargittai, I.; Brunvoll, J.; Kolonits, M.; Khodorkovsky, V. *J. Mol. Struc.* **1994**, *317*, 273.

(33) Liu, R.; Zhou, X.; Kasmai, H. *Spectrochim. Acta* **1997**, *A53*, 1241.

(34) Demiralp, E.; Goddard, W. A., III. *J. Phys. Chem. A* **1997**, *101*, 8128.

(35) Viruela, R.; Viruela, P. M.; Pou-Amérigo, R.; Ortí, E. *Synth. Met.* **1999**, *103*, 1991.

(36) Katan, C. *J. Phys. Chem. A* **1999**, *103*, 1407.

(37) Adamo, C.; Arnaud, R.; Scalmani, G.; Müller, H.; Sahli, F.; Barone, V. *J. Phys. Chem. B* **1999**, *103*, 6863.

(38) Yakushi, K.; Nishimura, S.; Sugano, T.; Kuroda, H.; Ikemoto, I. *Acta Cryst.* **1980**, *B36*, 358.

(39) Kistenmacher, T. J.; Rossi, M.; Chiang, C. C.; Van Duyne, R. P.; Siedle, A. R. *Inorg. Chem.* **1980**, *19*, 3604.

(40) Andersson, K.; Malmqvist, P.-Å.; Roos, B. O.; Sadlej, A. J.; Wolinski, K. *J. Phys. Chem.* **1990**, *94*, 5483.

(41) Andersson, K.; Malmqvist, P.-Å.; Roos, B. O. *J. Chem. Phys.* **1992**, *96*, 1218.

(42) Andersson, K.; Roos, B. O. Multiconfigurational second-order perturbation theory. In *Modern electron structure theory;* Yarkony, R., Ed.; Advanced Series in Physical Chemistry, Vol. 2, Part 1; World Scientific Publishing Co.: Singapore, 1995, pp 55−109.

(43) Finley, J.; Malmqvist, P.-Å.; Roos, B. O.; Serrano-Andrés, L. *Chem. Phys. Lett.* **1998**, *288*, 299.

(44) Rubio, M.; Roos, B. O. *Mol. Phys.* **1999**, *96*, 603.

(45) Crespo, R.; Merchán, M.; Michl, J. *J. Phys. Chem. A* **2000**, *104*, 8593.

(46) Molina, V.; Merchán, M. *J. Phys. Chem. A* **2001**, *105*, 3745.

(47) Molina, V.; Merchán, M. *Proc. Natl. Acad. Sci.* **2001**, *98*, 4299.

(48) Serrano-Andrés, L.; Merchán, M.; Borin, A. C.; Stålring, J. *Int. J. Quantum Chem.* **2001**, *84*, 181.

(49) Malmqvist, P.-Å. *Int. J. Quantum Chem.* **1986**, *30*, 479.

(50) Malmqvist, P.-Å.; Roos, B. O. *Chem. Phys. Lett.* **1989**, *155*, 189.

(51) Andersson, K.; Blomberg, M. R. A.; Fülscher, M. P.; Karlstöm, G.; Lindh, R.; Malmqvist, P.-Å.; Neogrády, P.; Olsen, J.; Roos, B. O.; Sadlej, A. J.; Schütz, M.; Seijo, L.; Serrano-Andrés, L.; Siegbahn, P. E. M.; Widmark, P.-O. *MOLCAS*, Version 4.0; Department of Theor. Chem., Chem. Center, University of Lund, P. O. B. 124, S-221 00: Lund, Sweden, 1997.

(52) Demiralp, E.; Dasgupta, S.; Goddard, W. A., III. *J. Am. Chem. Soc.* **1995**, *117*, 8154.

(53) Cooper, W. F.; Kenney, N. C.; Edmonds, J. W.; Nagel, A.; Wudl, F.; Coppens, P. *J. Chem. Soc., Chem. Commun.* **1971**, 889.

(54) Cooper, W. F.; Edmonds, J. W.; Wudl, F.; Coppens, P. *Cryst. Struct. Commun.* **1974**, *3*, 23.

(55) Ellern, A.; Bernstein, J.; Becker, J. Y.; Zamir, S.; Shahal, L.; Cohen, S. *Chem. Mater.* **1994**, *6*, 1378.

(56) Wang, C.; Bryce, M. R.; Batsanov, A. S.; Howard, J. A. K. *Chem. Eur. J.* **1997**, *3*, 1679.

(57) Bak, B.; Christensen, D.; Hansen-Nygaard, L.; Rastrup-Andersen, J. *J. Mol. Spectrosc.* **1961**, *7*, 58.

(58) Hünig, S.; Kieβlich, G.; Quast, H.; Scheutzow, D. *Liebigs Ann. Chem.* **1973**, 310.
(59) Klots, C. E.; Compton, R. N.; Raaen, V. F. *J. Chem. Phys.* **1974**, *60*, 1177.
(60) Wudl, F.; Kruger, A. A.; Kaplan, M. L.; Hutton, R. S. *J. Org. Chem.* **1977**, *42*, 768.
(61) Engler, E. M.; Scott, B. A.; Etemad, S.; Penney, T.; Patel, V. V. *J. Am. Chem. Soc.* **1977**, *99*, 5909.
(62) Sandman, D. J.; Holmes, T. J.; Warner, D. E. *J. Org. Chem.* **1979**, *44*, 880.
(63) Gleiter, R.; Schmidt, E.; Cowan, D. O.; Ferraris, J. P. *J. Electron Spectrosc. Relat. Phenom.* **1973**, *2*, 207.
(64) Gleiter, R.; Kobayashi, M.; Spanget-Larsen, J.; Ferraris, J. P.; Bloch, A. N.; Bechgaard, K.; Cowan, D. O. *Ber. Bunsen-Ges. Phys. Chem.* **1975**, *79*, 1218.
(65) Wudl, F.; Smith, G. M.; Hufnagel, E. J. *J. Chem. Soc., Chem. Commun.* **1970**, 1453.
(66) Torrance, J. B.; Scott, B. A.; Welber, B.; Kaufman, F. B.; Seiden, P. E. *Phys. Rev. B* **1979**, *19*, 730.
(67) Bozio, R.; Zanon, I.; Girlando, A.; Pecile, C. *J. Chem. Phys.* **1979**, *71*, 2282.
(68) Sugano, T.; Yakushi, K.; Kuroda, H. *Bull. Chem. Soc. Jpn.* **1978**, *51*, 1041.
(69) Berlinsky, A. J.; Carolan, J. F.; Weiler, L. *Can. J. Chem.* **1974**, *52*, 3373.
(70) Lichtenberger, D. L.; Johnston, R. L.; Hinkelmann, K.; Suzuki, T.; Wudl, F. *J. Am. Chem. Soc.* **1990**, *112*, 3302.
(71) Rubio, M.; Merchán, M.; Ortí, E.; Roos, B. O. *J. Phys. Chem.* **1995**, *99*, 14980.
(72) Teitelbaum, R. C.; Marks, T. J.; Johnson, C. K. *J. Am. Chem. Soc.* **1980**, *102*, 2986.
(73) Matsubayashi, G.; Ueyama, K.; Tanaka, T. *J. Chem. Soc., Dalton Trans.* **1985**, 465.